Convolutional Neural Network for Accurate Analysis of Methamphetamine with Upconversion Lateral Flow Biosensor

Lei Huang, Shulin Tian, Wenhao Zhao, Ke Liu[ID], Xing Ma and Jinhong Guo[ID]

***Abstract*—Methamphetamine is a powerful stimulant drug, the abuse of which threatens human health and social stability. Rapid and accurate quantification of methamphetamine is essential to inhibit the abuse and prevalence of methamphetamine effectively. In this paper, we present a portable fluorescence reader with upconverting nanoparticle-labeled lateral flow immunoassay (LFIA) for rapid and accurate quantification of methamphetamine. Based on specific binding of a methamphetamine antigen to an antibody in the LFIA, the fluorescence reader is designed to capture and record the fluorescence intensities T and C of the test and control lines, respectively, and the T/C ratio is calculated to determine the concentration of methamphetamine. The linear range for methamphetamine is 0.1–100 ng/mL. Because the sensor is often susceptible to noise interference, using only the T/C ratio to distinguish weakly positive and negative samples of methamphetamine renders the results inaccurate. To solve this problem, we applied a convolutional neural network (CNN) to learn image features of different methamphetamine concentrations (0, 0.01, 0.05, 0.1, and 0.5 ng/mL) for accurate detection of weakly positive and negative samples. The results show that the proposed method can effectively detect weakly positive and negative samples of methamphetamine with an accuracy of up to 92%. The CNN provides a novel scheme for accurate analysis of weakly positive and negative samples in upconverting nanoparticle-labeled LFIA.**

***Index Terms*—Convolutional neural network, fluorescence reader, lateral flow immunoassay, upconverting nanoparticle**

Manuscript received on November 15, 2021. (Corresponding authors: Ke Liu; Jinhong Guo.)

L. Huang is with the School of Automation Engineering, University of Electronic School and Technology of China, Chengdu 611731, China (email: 18200279388@163.com).

S. Tian is with the School of Automation Engineering, University of Electronic School and Technology of China, Chengdu 611731, China (email: shulin@uestc.edu.cn).

W. Zhao is with the School of Automation Engineering, University of Electronic School and Technology of China, Chengdu 611731, China (email: vinhou@163.com).

K. Liu is with the School of Automation Engineering, University of Electronic School and Technology of China, Chengdu 611731, China (email: liuke@uestc.edu.cn).

X. Ma is with the School of Materials Science and Engineering, Harbin Institute of Technology (Shenzhen), Shenzhen 518055, China. He is also with the Shenzhen Bay Laboratory, No.9 Duxue Road, Shenzhen 518055, China (email: maxing@hit.edu.cn).

J. Guo is with the School of Information and Communication Engineering, University of Electronic Science and Technology of China, Chengdu 611731, China (e-mail: guojinhong@uestc.edu.cn).

I. Introduction

METHAMPHETAMINE is a powerful stimulant drug that can strongly stimulate the central nervous system and cause irreparable damage to human health.[1-3] Currently, the number of people who abuse methamphetamine is increasing rapidly, resulting in serious social problems, such as violent behavior and criminal activity.[4-6] According to *Drug Situation in China (2019)*, methamphetamine has become the most abused illicit drug in China (http://www.nncc626.com/2020-06/25/c_1210675877.htm). To effectively inhibit the abuse and prevalence of methamphetamine, tests for the rapid and accurate quantification of methamphetamine have gained considerable attention in recent years. The methods usually used to detect methamphetamine include gas, liquid, or high-performance liquid chromatography-tandem mass spectrometry.[7-11] Although these methods have outstanding advantages of high specificity and sensitivity, they require not only a complicated sample pretreatment process but also well-trained personnel to operate expensive large-scale instruments, making them unsuitable for point-of-care testing.[12, 13]

The lateral flow immunoassay (LFIA), which is designed to detect target analytes in a given sample (with a size of dozens of milliliters) is extremely suitable for point-of-care testing, because of its simplicity, portability, cost-effectiveness, and rapid detection.[14-19] Therefore, LFIA has been applied in a variety of fields, including clinical analysis, food safety, and environmental monitoring.[20-22] Usually, the LFIA utilizes gold nanoparticles as labels, owing to the easy sample preparation and visual detection.[23, 24] However, LFIA based on gold nanoparticles often has drawbacks; the sensitivity is low and semi-quantification is usually available.[25] To improve sensitivity and obtain quantitative detection results, upconverting nanoparticles (UCNPs) that can convert low-energy infrared excitation light into high-energy visible light, have been applied as LFIA labels instead.[26-28] In addition, UCNPs with a large anti-Stokes shift have the advantages of low background autofluorescence levels and high signal-to-noise ratio.[29-33]

In this study, a fluorescence quantification method was developed, which involved analyzing fluorescence signals from UCNPs to obtain quantitative results. In this approach, the

upconversion luminescence signal distribution of the UCNPs on the LFIA is measured, and the ratio of the upconversion luminescence signal in the test line to that in the control line is utilized as the detection result. For example, Yan *et al*.[34] reported a UCNP-based biosensor for rapid detection of *Yersinia pestis*. In this biosensor, a dichroic mirror was used to reflect 980 nm infrared light on the LFIA surface and excite the UCNPs. Using the same dichroic mirror, the excited light could be transmitted to a photomultiplier tube. However, it was quite difficult to accurately align and assemble the optical system. Subsequently, Huang *et al*.[35] reported a UCNP-based biosensor using a simplified optical system for rapid detection of *Yersinia pestis*. However, Huang *et al*.[35] still opted to use a photomultiplier tube as a receiver; this rendered their system bulky and expensive, making it unfavorable for point-of-care testing.

With the rapid development of artificial intelligence, machine learning and deep learning have been widely applied in medical detection. For example, Yan *et al*.[36] proposed a support vector machine to accurately analyze the weak magnetic signal from magnetic nanoparticles used as labels in an LFIA to classify weakly positive and negative samples of human chorionic gonadotropin to improve sensitivity. In this assay, concentrations of 0 and 0.25 mIU/mL were set as negative, whereas concentrations of 0.5, 1, 2.5, 5, and 10 mIU/mL were set as positive. Although the accuracy of the support vector machine classifier was 100%, it was still unable to detect these different concentrations accurately. Zeng *et al*.[37] used a convolutional neural network (CNN) to extract test and control lines of an LFIA based on gold nanoparticles for the quantitative analysis of human chorionic gonadotropin. However, artificially labeling specific areas of acquired images as background and specimen might have a negative impact on the test results.

In this paper, we present a portable fluorescence reader with UCNP-labeled LFIA for the rapid and accurate quantification of methamphetamine. Based on specific binding of the methamphetamine antigen to an antibody on the LFIA, the fluorescence reader is designed to capture and record the fluorescence intensities T and C of the test and control lines, respectively, and the T/C ratio is calculated to determine the concentration of methamphetamine. The linear range for methamphetamine in this sensor is 0.1–100 mg/mL. However, if only the T/C ratio is used to distinguish weakly positive and negative samples of methamphetamine, the sensor is often susceptible to noise interference, making the test results inaccurate. To solve this problem, we employed a CNN to learn image features of different methamphetamine concentrations (0, 0.01, 0.05, 0.1, and 0.5 ng/mL) for accurate detection of weakly positive and negative samples. The results show that the proposed sensor can effectively detect weakly positive and negative samples of methamphetamine with an accuracy of up to 92%. Moreover, the CNN provides a novel scheme for accurate analysis of weakly positive and negative samples in this UCNP-based LFIA.

II. Theory And Methods

A. Upconversion Lateral Flow Biosensor

Generally, the LFIA consists of four parts, namely, a sample pad, a conjugate pad, a nitrocellulose membrane, and an absorbent pad. These parts are integrated in a backing card with appropriate overlaps, as shown in Fig. 1(a). The sample of interest is loaded onto the sample pad and is transported to other parts of the LFIA by capillary action. The conjugate pad is utilized to disperse UCNP-labeled antibody (UCNP–Ab) and UCNP-labeled reference antibody (UCNP–rabbit immunoglobulin G [IgG]). The nitrocellulose membrane immobilizes the methamphetamine bovine serum albumin (BSA) conjugant (MET–BSA) and goat anti-rabbit IgG as the test and control lines, respectively. The absorbent pad drives the capillary action and prevents backflow of the loaded sample.

Based on the specific binding of the methamphetamine antigen to the antibody, methamphetamine with a single epitope can be detected using the competitive action of the LFIA, as shown in Fig. 1(b). If a sample containing antigen is loaded on the sample pad, the antigen initially reacts with the UCNP–Ab on the conjugate pad to form a UCNP–Ab/antigen complex; any unreacted UCNP–Ab is captured by the MET–BSA on the test line to form a UCNP–Ab/MET–BSA complex. While a decrease in the amount of antigen in the sample, more unreacted UCNP–Ab is captured by the MET–BSA, resulting in a larger quantity of UCNPs on the test line than is obtained for a methamphetamine-positive sample. Therefore, the fluorescence intensity of the test line is inversely proportional to the concentration of methamphetamine. Because the UCNP–rabbit IgG conjugate binds independently to the goat anti-rabbit IgG, the fluorescence intensity of the control line is not influenced by the concentration of antigen; a visible signal from the control line indicates proper functioning of the LFIA.

To accomplish quantitative analysis of methamphetamine, a fluorescence reader was designed to record and calculate the fluorescence intensities of the test and control lines. The fluorescence reader mainly consists of a photoelectric measurement system and a control system, as shown in Fig. 2(a).

The photoelectric measurement system usually includes an illumination unit, an imaging unit, a scanning unit, and a complementary metal–oxide semiconductor (CMOS) camera. In the illumination unit, a light-emitting diode (LED) with a wavelength of 980 nm was selected to excite the UCNPs captured on the LFIA. As shown in Fig. 2(b), a lens is used to focus the infrared light beam into a rectangular focal line, 3 mm long by 1 mm wide. The optical axis of the illumination unit is inclined at 45° to the LFIA surface. In the imaging unit, a filter is utilized to filter out stray light, suppress background noise, and retain the fluorescence signals emitted from the UCNPs. Subsequently, a lens focuses the fluorescence signals for imaging. The optical axis of the imaging unit is perpendicular to the surface of the LFIA. The scanning unit contains a customized guide rail and a stepping motor. The LFIA placed on the guide rail is driven by the motor at constant velocity along the LFIA. A CMOS camera integrated with an operational amplifier, an analog to digital converter (ADC), and a differential amplifier are arranged behind the imaging unit to capture and record the distribution image of the fluorescence signals.

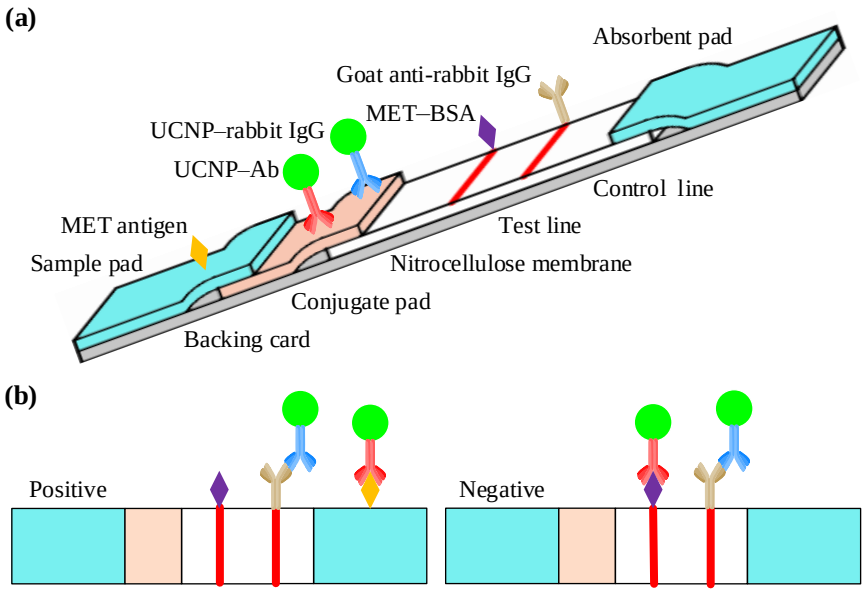

Fig. 1. UCNP-labeled LFIA: (a) layout; (b) competitive action. MET, methamphetamine.

The control system mainly contains a core STM32F103RB microcontroller unit (MCU). In addition to controlling the illumination and scanning units, the MCU drives the CMOS camera to record the fluorescence signals and process the camera output signal to obtain the detection results. Specifically, the fluorescence signals obtained using the CMOS camera are initially amplified by the operational amplifier and then converted into digital signals by the ADC. To eliminate the direct current (DC) component contained in the digital signals, a DC signal with an adjustable level was superimposed on the noninverting input of the differential amplifier. After the signal conversion was completed, the obtained data were fed back to the MCU for processing and analysis. Using signal processing algorithms, the fluorescence intensities of the test and control line are calculated by integrating the peak signals generated during the LFIA movement. Finally, the methamphetamine concentration is expressed as the fluorescence intensity of the test line relative to that of the control line (the T/C ratio).

B. Principle of CNN

In the competitive format of the LFIA, a smaller concentration of methamphetamine leads to a stronger fluorescence intensity on the test line, resulting in a higher T/C ratio. However, if only the T/C ratio is used to distinguish weakly positive and negative samples of methamphetamine, the LFIA is often susceptible to noise interference, making the test results inaccurate. Therefore, powerful fluorescence signal processing algorithms are required to classify weakly positive and negative samples. In the biological vision system, certain cells are only sensitive to a part of what they observe, thus forming visual information. Inspired by the visual system, the CNN known as a feedforward neural network is proposed for image processing. A typical CNN consists of a convolutional layer, a pooling layer, and a fully connected layer.

The convolutional layer can extract local features of input images using a convolution kernel with its own weight and bias value. Figure 3(a) shows the principle of the convolutional layer. Taking this image as an example, the convolution kernel performs a convolution operation with the input image (red solid line) to obtain a feature map of the convolutional layer (red dotted line). Because the convolution kernel is a sliding window, it begins to slide until the final feature map of the convolutional layer (blue dotted line) is obtained. In the whole process, a total of 16 convolution operations have been performed to obtain 16 feature maps, covering the initial input image.

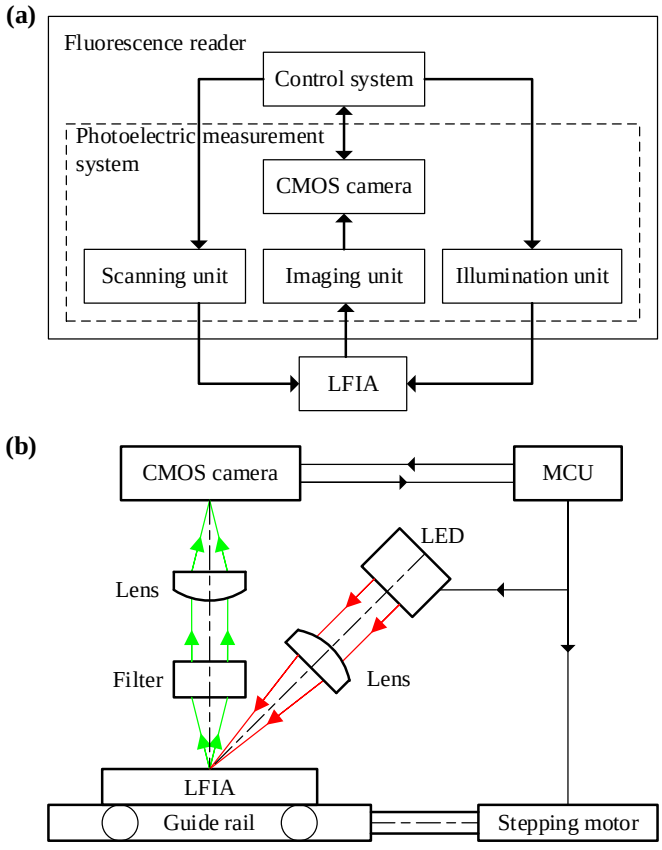

Fig. 2. Fluorescence reader: (a) composition; (b) layout.

Generally, a pooling layer follows the convolutional layer; the pooling layer is applied to reduce the quantity of data and prevent overfitting. There are two types of pooling layer: maximum pooling and average pooling. Figure 3(b) shows an example of a pooling layer, where a subsampling operation is applied to reduce the size of the convolutional layer by half and obtain the feature maps of the pooling layer. Specifically, the maximum value is selected for the feature map of the maximum pooling layer, whereas the average value is selected for the feature map of the average pooling layer. Finally, the fully connected layer is applied to connect all the extracted features and generate a classifier to output the results.

III. Results And Discussion

A. Performance of Upconversion Lateral Flow Biosensor

In evaluating the performance of a fluorescence reader, it is important to assess its sensitivity. We selected the ratio of the fluorescence intensities of the test and control lines, T/C, as a measure of methamphetamine concentration, to effectively eliminate differences between different LFIAs. To obtain a standard curve, different concentrations of methamphetamine antigen (0.1, 0.5, 1, 5, 10, 50, and 100 ng/mL) were prepared to determine the correlation between the T/C ratio and the methamphetamine concentration; three LFIAs were prepared for each concentration and each concentration was evaluated three times under the same conditions. Figure 4 shows an example of the fluorescence intensities corresponding to 0, 0.1, 0.5, 1, 5, 10, 50, and 100 ng/mL methamphetamine, respectively. The average value and standard deviation were calculated as the final concentration and error, respectively. As shown in Fig. 5(a), the logarithm of the methamphetamine concentration and the T/C ratio have a linear relationship. The linear range for methamphetamine is 0.1–100 ng/mL.[38]

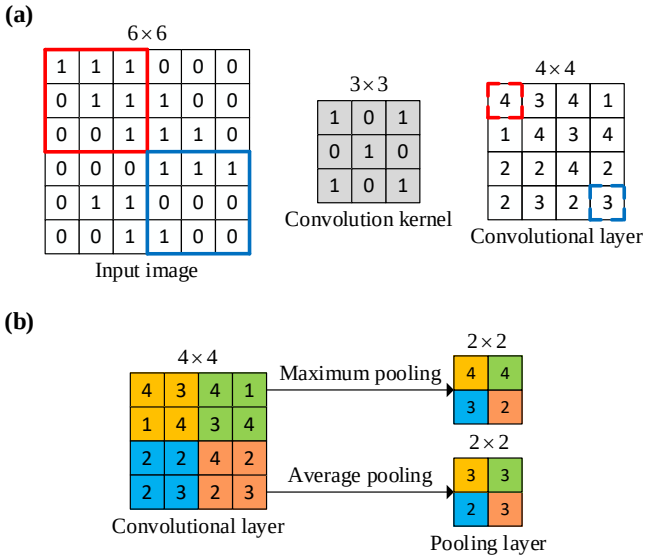

Fig. 3. Principle of CNN: (a) convolutional layer; (b) pooling layer.

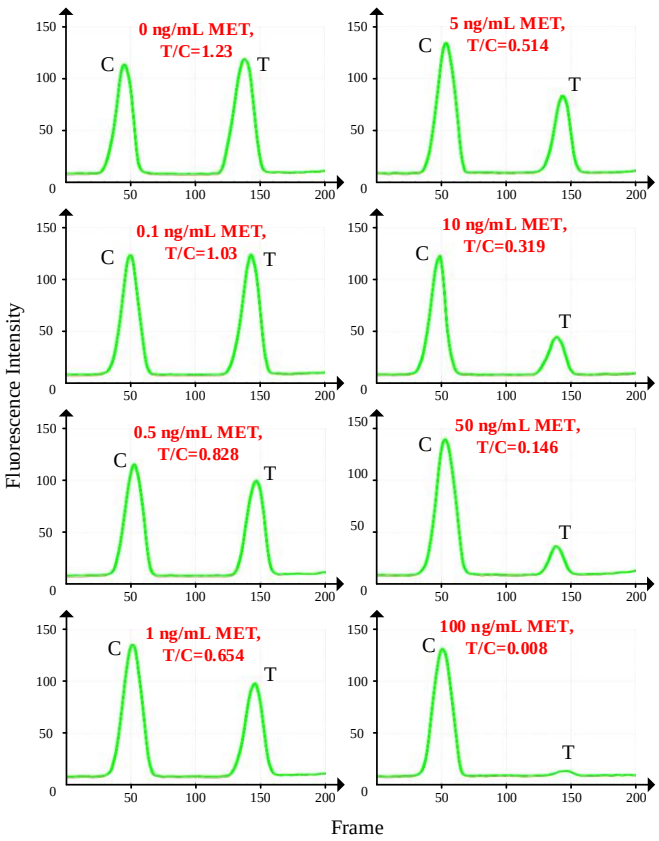

Fig. 4. Examples of fluorescence intensities corresponding to 0, 0.1, 0.5, 1, 5, 10, 50, and 100 ng/mL methamphetamine, respectively.

Random errors can be caused by different settings. The quality of repeatability relates to the consistency of repeated measurement results under the same conditions. In this assay, three concentrations of methamphetamine (0.5, 5, and 50 ng/mL) were used to determine system repeatability; a single LFIA was prepared for each concentration and each LFIA was evaluated 20 times. The system repeatability was evaluated by calculating the coefficient of variation (CV), which is equal to the ratio of the standard deviation and the average detected value. A lower CV indicates better stability and repeatability. As shown in Table 1, the maximum CV for the system was 3.73%, indicating good repeatability of the fluorescence reader.

To assess the reliability of the fluorescence reader, 25 clinical samples were measured using high-performance liquid chromatography mass spectrometry (HPLC-MS) and a fluorescence reader. As shown in Fig. 5(b), a strong linear correlation was obtained between the two methods, indicating the reliability of the fluorescence reader for quantification of methamphetamine.[38]

TABLE 1
MEASURED METHAMPHETAMINE CONCENTRATIONS CONTAINING LOW, MEDIUM, AND HIGH LEVELS.

Standard concentration	Low (0.5 ng/mL)	Medium (5 ng/mL)	High (50 ng/mL)
Number of measurements	20	20	20
Average measured concentration (ng/mL)	0.503	5.010	49.915
Standard deviation	0.013	0.187	1.617
Coefficient of variation (%)	2.66	3.73	3.24

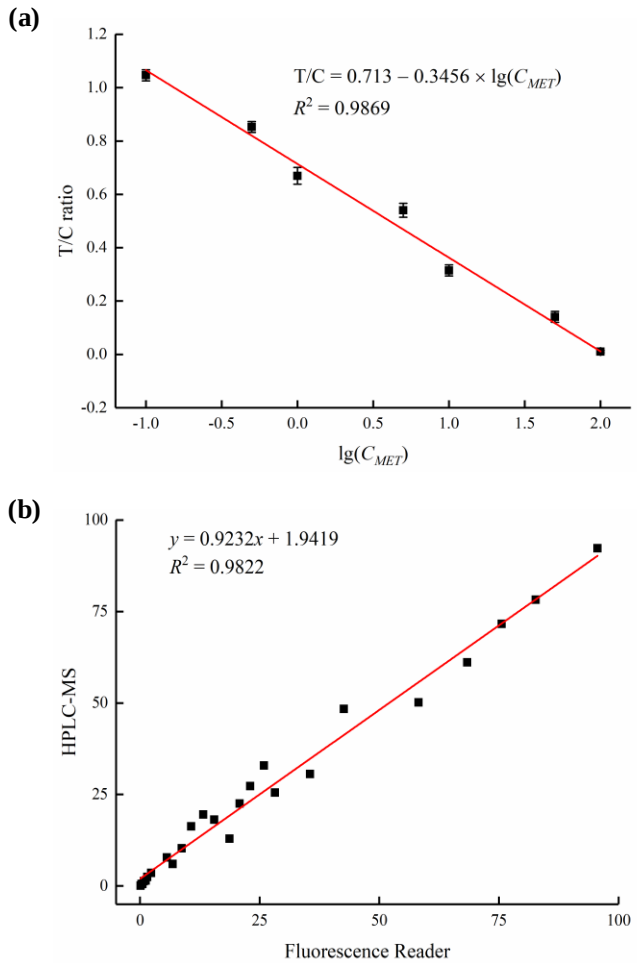

Fig. 5. (a) Linear relationship between methamphetamine concentration and T/C ratio (Fig. 2A in reference 38); (b) comparison between HPLC-MS and fluorescence reader for detection of methamphetamine (Fig. 2B in reference 38).

B. CNN for Accurate Analysis of Methamphetamine

Although the upconversion lateral flow biosensor has achieved good performance in the detection of methamphetamine, it is often susceptible to noise interference if only the T/C ratio is used to distinguish weakly positive and negative samples (0, 0.01, 0.05, 0.1, and 0.5 ng/mL methamphetamine), as shown in Fig. 6. Therefore, there is classification task: to distinguish weakly positive and negative samples, where five concentrations of methamphetamine correspond to five labels.

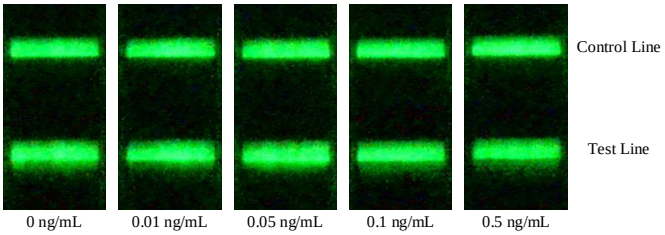

Fig. 6. Example of fluorescence images for five different concentrations of methamphetamine.

The proposed CNN consists of an input layer, two convolutional layers, two pooling layers, two fully connected layers, and an output layer, as shown in Fig. 7. All training images were resized to 240 × 240 pixels with three channels. The first convolutional (C1) layer had six convolution kernels of size 5 × 5, so the output of this layer contained 6 × 240 × 240 feature maps. Following the first convolutional layer, the first maximum pooling (S1) layer of size 2 × 2 was employed to reduce the dimensions and give 6 × 120 × 120 feature maps. Similarly, the second convolutional (C2) layer had 16 convolution kernels of size 5 × 5; thus, the output of this layer contained 16 × 120 × 120 feature maps. Subsequently, the second maximum pooling (S2) layer of size 4 × 4 was utilized to reduce the dimensions and give 16 × 30 × 30 feature maps. Finally, two fully connected (FC1 and FC2) layers were used to generate a classifier with five outputs. The appropriate parameters selected in the CNN model are given in Table II.

In this study, a total of 600 images with five different concentrations of methamphetamine were selected to verify the feasibility of the proposed CNN model, where 120 images were output for each concentration. Specifically, we randomly selected 400 images as the training group, and the remaining 200 images as the testing group. Figure 8 shows the performance of the CNN model, with accuracy up to 92%. Therefore, the proposed CNN model is a reliable method for accurately distinguishing weakly positive and negative samples.

TABLE II
CRUCIAL PARAMETERS USED IN THE CNN MODEL

CNN parameters	Setting
Epoch	80
Batch size	64
Activation function	ReLU
Optimizer	Adam
Loss function	Cross entropy
Learning rate	0.001

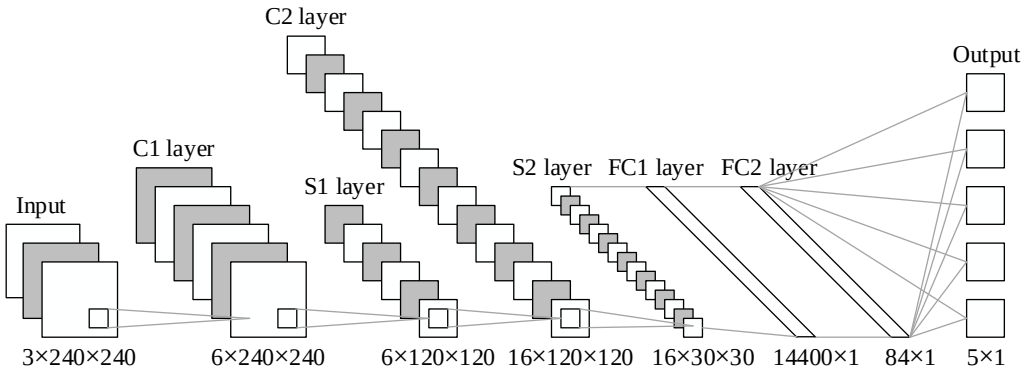

Fig. 7. Structure of proposed CNN model.

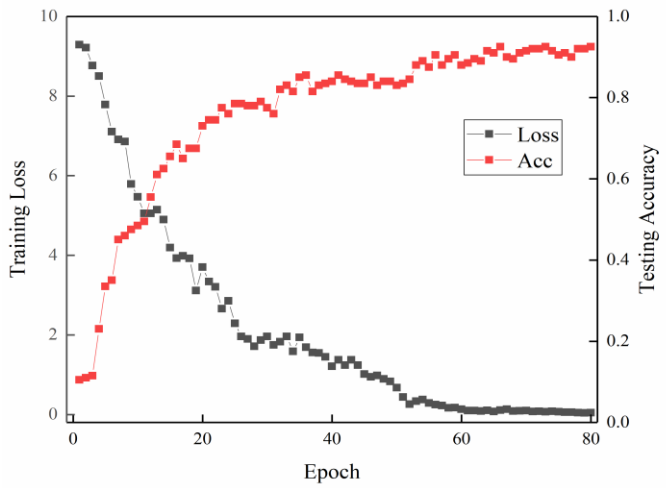

Fig. 8. Performance of the proposed CNN model.

IV. Conclusion

In this paper, we propose a portable fluorescence reader with UCNP-labeled LFIA for rapid and accurate quantification of methamphetamine. The methamphetamine concentration is quantified based on the fluorescence intensities of the test and control lines on the LFIA. The quantitative detection range for methamphetamine is 0.1–100 ng/mL. A CNN algorithm is then applied to detect different methamphetamine concentrations (0, 0.01, 0.05, 0.1, and 0.5 ng/mL) for accurate detection of weakly positive and negative samples, to improve the accuracy of the sensor. We envision that this type of fluorescence reader with a UCNP-labeled LFIA can be easily adapted for other applications, such as food analysis, environmental monitoring, and national security. The CNN also provides a novel scheme for the accurate analysis of weakly positive and negative samples in UCNP-based LFIA.

References

[1] A. Choodum, P. Kanatharana, W. Wongniramaikul, and N. NicDaeid, "A sol–gel colorimetric sensor for methamphetamine detection," *Sensors and Actuators B: Chemical*, vol. 215, pp. 553-560, 2015/08/01/ 2015.

[2] Y. Zhang, B. R. Bunes, N. Wu, A. Ansari, S. Rajabali, and L. Zang, "Sensing methamphetamine with chemiresistive sensors based on polythiophene-blended single-walled carbon nanotubes," *Sensors and Actuators B: Chemical*, vol. 255, pp. 1814-1818, 2018/02/01/ 2018.

[3] M. Akhoundian, T. Alizadeh, M. R. Ganjali, and P. Norouzi, "Ultra-trace detection of methamphetamine in biological samples using FFT-square wave voltammetry and nano-sized imprinted polymer/MWCNTs -modified electrode," *Talanta*, vol. 200, pp. 115-123, 2019/08/01/ 2019.

[4] S. Rouhani and S. Haghgoo, "A novel fluorescence nanosensor based on 1,8-naphthalimide-thiophene doped silica nanoparticles, and its application to the determination of methamphetamine," *Sensors and Actuators B: Chemical*, vol. 209, pp. 957-965, 2015/03/31/ 2015.

[5] K. Mao, Z. Yang, J. Li, X. Zhou, X. Li, and J. Hu, "A novel colorimetric biosensor based on non-aggregated Au@Ag core–shell nanoparticles for methamphetamine and cocaine detection," *Talanta*, vol. 175, pp. 338-346, 2017/12/01/ 2017.

[6] X. Sun *et al.*, "Methamphetamine produces cardiac damage and apoptosis by decreasing melusin," *Toxicology and Applied Pharmacology*, vol. 378, p. 114543, 2019/09/01/ 2019.

[7] E. Han *et al.*, "Relationship between methamphetamine use history and segmental hair analysis findings of MA users," *Forensic Science International*, vol. 254, pp. 59-67, 2015/09/01/ 2015.

[8] N. Suwannachom, T. Thananchai, A. Junkuy, T. E. O'Brien, and P. Sribanditmongkol, "Duration of detection of methamphetamine in hair after abstinence," *Forensic Science International*, vol. 254, pp. 80-86, 2015/09/01/ 2015.

[9] I. Shu, A. Alexander, M. Jones, J. Jones, and A. Negrusz, "Determination of methamphetamine enantiomer composition in human hair by non-chiral liquid chromatography–tandem mass spectrometry method," *Journal of Chromatography B*, vol. 1028, pp. 145-152, 2016/08/15/ 2016.

[10] T. Wang *et al.*, "Disappearance of R/S-methamphetamine and R/S-amphetamine from human scalp hair after discontinuation of methamphetamine abuse," *Forensic Science International*, vol. 284, pp. 153-160, 2018/03/01/ 2018.

[11] J. Ou *et al.*, "An evaluation of the cut-off value of methamphetamine in hair samples via HPLC-MS/MS," *Forensic Science International*, vol. 306, p. 110094, 2020/01/01/ 2020.

[12] E. B. Bahadır and M. K. Sezgintürk, "Lateral flow assays: Principles, designs and labels," *TrAC Trends in Analytical Chemistry*, vol. 82, pp. 286-306, 2016/09/01/ 2016.

[13] L.-M. Hu *et al.*, "Advantages of time-resolved fluorescent nanobeads compared with fluorescent submicrospheres, quantum dots, and colloidal gold as label in lateral flow assays for detection of ractopamine," *Biosensors and Bioelectronics*, vol. 91, pp. 95-103, 2017/05/15/ 2017.

[14] D. Quesada-González and A. Merkoçi, "Nanoparticle-based lateral flow biosensors," *Biosensors and Bioelectronics*, vol. 73, pp. 47-63, 2015/11/15/ 2015.

[15] Y. Chen *et al.*, "Near-infrared fluorescence-based multiplex lateral flow immunoassay for the simultaneous detection of four antibiotic residue families in milk," *Biosensors and Bioelectronics*, vol. 79, pp. 430-434, 2016/05/15/ 2016.

[16] T. Mahmoudi, M. de la Guardia, B. Shirdel, A. Mokhtarzadeh, and B. Baradaran, "Recent advancements in structural improvements of lateral flow assays towards point-of-care testing," *TrAC Trends in Analytical Chemistry*, vol. 116, pp. 13-30, 2019/07/01/ 2019.

[17] L. Huang, S. Tian, W. Zhao, K. Liu, X. Ma, and J. Guo, "Multiplexed detection of biomarkers in lateral-flow immunoassays," *Analyst*, vol. 145, no. 8, pp. 2828-2840, Apr 21 2020.

[18] L. Huang, S. Tian, W. Zhao, K. Liu, X. Ma, and J. Guo, "Aptamer-based lateral flow assay on-site biosensors," *Biosensors and Bioelectronics*, p. 113279, 2021/04/24/ 2021.

[19] W. Zhao, S. Tian, L. Huang, K. Liu, L. Dong, and J. Guo, "A smartphone-based biomedical sensory system," *Analyst*, vol. 145, no. 8, pp. 2873-2891, Apr 21 2020.

[20] V.-T. Nguyen, S. Song, S. Park, and C. Joo, "Recent advances in high-sensitivity detection methods for paper-based lateral-flow assay," *Biosensors and Bioelectronics*, vol. 152, p. 112015, 2020/03/15/ 2020.

[21] Z. Gao *et al.*, "Platinum-Decorated Gold Nanoparticles with Dual Functionalities for Ultrasensitive Colorimetric in Vitro Diagnostics," *Nano Letters*, vol. 17, no. 9, pp. 5572-5579, 2017/09/13 2017.

[22] K. Zhang, J. Wu, Y. Li, Y. Wu, T. Huang, and D. Tang, "Hollow nanogold microsphere-signalized lateral flow immunodipstick for the sensitive determination of the neurotoxin brevetoxin B," *Microchimica Acta*, vol. 181, no. 11, pp. 1447-1454, 2014/08/01 2014.

[23] W. C. Mak, V. Beni, and A. P. F. Turner, "Lateral-flow technology: From visual to instrumental," *TrAC Trends in Analytical Chemistry*, vol. 79, pp. 297-305, 2016/05/01/ 2016.

[24] W. Xiao *et al.*, "A simple and compact smartphone-based device for the quantitative readout of colloidal gold lateral flow immunoassay strips," *Sensors and Actuators B: Chemical*, vol. 266, pp. 63-70, 2018/08/01/ 2018.

[25] X. Huang, Z. P. Aguilar, H. Xu, W. Lai, and Y. Xiong, "Membrane-based lateral flow immunochromatographic strip with nanoparticles as reporters for detection: A review," *Biosensors and Bioelectronics*, vol. 75, pp. 166-180, 2016/01/15/ 2016.

[26] L. Lei, J. Zhu, G. Xia, H. Feng, H. Zhang, and Y. Han, "A rapid and user-friendly assay to detect the Neutrophil gelatinase-associated

lipocalin (NGAL) using up-converting nanoparticles," *Talanta*, vol. 162, pp. 339-344, 2017/01/01/ 2017.

[27] Z. Zhang, S. Shikha, J. Liu, J. Zhang, Q. Mei, and Y. Zhang, "Upconversion Nanoprobes: Recent Advances in Sensing Applications," *Analytical Chemistry*, vol. 91, no. 1, pp. 548-568, Jan 1 2019.

[28] B. Jin *et al.*, "Lateral flow aptamer assay integrated smartphone-based portable device for simultaneous detection of multiple targets using upconversion nanoparticles," *Sensors and Actuators B: Chemical*, vol. 276, pp. 48-56, 2018/12/10/ 2018.

[29] Z. Luo, Q. Qi, L. Zhang, R. Zeng, L. Su, and D. Tang, "Branched Polyethylenimine-Modified Upconversion Nanohybrid-Mediated Photoelectrochemical Immunoassay with Synergistic Effect of Dual-Purpose Copper Ions," *Analytical Chemistry*, vol. 91, no. 6, pp. 4149-4156, 2019/03/19 2019.

[30] Z. Luo, L. Zhang, R. Zeng, L. Su, and D. Tang, "Near-Infrared Light-Excited Core–Core–Shell UCNP@Au@CdS Upconversion Nanospheres for Ultrasensitive Photoelectrochemical Enzyme Immunoassay," *Analytical Chemistry*, vol. 90, no. 15, pp. 9568-9575, 2018/08/07 2018.

[31] Z. Qiu, J. Shu, and D. Tang, "Near-Infrared-to-Ultraviolet Light-Mediated Photoelectrochemical Aptasensing Platform for Cancer Biomarker Based on Core–Shell NaYF4:Yb,Tm@TiO2 Upconversion Microrods," *Analytical Chemistry*, vol. 90, no. 1, pp. 1021-1028, 2018/01/02 2018.

[32] Z. Qiu, J. Shu, and D. Tang, "NaYF4:Yb,Er Upconversion Nanotransducer with in Situ Fabrication of Ag2S for Near-Infrared Light Responsive Photoelectrochemical Biosensor," *Analytical Chemistry*, vol. 90, no. 20, pp. 12214-12220, 2018/10/16 2018.

[33] Z. Qiu, J. Shu, J. Liu, and D. Tang, "Dual-Channel Photoelectrochemical Ratiometric Aptasensor with up-Converting Nanocrystals Using Spatial-Resolved Technique on Homemade 3D Printed Device," *Analytical Chemistry*, vol. 91, no. 2, pp. 1260-1268, 2019/01/15 2019.

[34] Z. Yan *et al.*, "Rapid quantitative detection of Yersinia pestis by lateral-flow immunoassay and up-converting phosphor technology-based biosensor," *Sensors and Actuators B: Chemical*, vol. 119, no. 2, pp. 656-663, 2006/12/07/ 2006.

[35] L. Huang *et al.*, "A Simple Optical Reader for Upconverting Phosphor Particles Captured on Lateral Flow Strip," *IEEE Sensors Journal*, vol. 9, no. 10, pp. 1185-1191, 2009.

[36] W. Yan, K. Wang, H. Xu, X. Huo, Q. Jin, and D. Cui, "Machine Learning Approach to Enhance the Performance of MNP-Labeled Lateral Flow Immunoassay," *Nano-Micro Letters*, vol. 11, no. 1, Jan 17 2019, Art. no. 7.

[37] N. Zeng, H. Li, Y. Li, and X. Luo, "Quantitative Analysis of Immunochromatographic Strip Based on Convolutional Neural Network," *IEEE Access*, vol. 7, pp. 16257-16263, 2019.

[38] L. Huang, S. Tian, W. Zhao, K. Liu, X. Ma, and J. Guo, "Highly Sensitive Detection of MET Using Support Vector Machine on a Portable Fluorescent Analyzer with UCNP-based Lateral Flow Assay," *MicroTAS 2021 Conference*, 10-14 Oct 2021.